An Effective Mesh Strategy for CFD Modelling of Polymer Electrolyte Membrane Fuel Cells

P. Choopanya*, Z. Yang[1]
National Metal and Materials Technology Center (MTEC), 114 Thailand Science Park (TSP), Pathum Thani, 12120, Thailand
[1]Department of Engineering, College of Engineering and Technology, University of Derby, Derby, United Kingdom DE22 3AW
*corresponding author. Email: pattarapong.cho@mtec.or.th

Highlights

- A PEM fuel cell-specific mesh strategy is proposed for the first time.
- The mesh in each direction has unequal influence on the solutions.
- Computation time is reduced considerably while good accuracy is maintained.
- The proposed mesh is valid over a wide range of cell sizes and flow-fields.

Abstract

Computational fluid dynamics (CFD) is a major tool in PEM fuel cell research. Typical three-dimensional PEM fuel cell models involve more than 10^6 mesh elements. This makes the computation very intense and necessitates a methodology to mesh the computational domain that can keep the number of elements to a minimum while maintaining good accuracy. In this study, the effect of computational mesh in each direction on the accuracy of the solution is investigated in a systematic way. It is found that the mesh in different directions has a different degree of influence on the solution suggesting that the mesh in one direction can be coarser than the other. The proposed mesh strategy is capable of greatly reducing the number of mesh elements, hence computation time, while preserving the characteristics of important flow-field variables. Moreover, it is applicable to a wide range of cell sizes and flow-field configurations and should be used as a guideline for mesh generation.

Keywords: PEM fuel cell, CFD, modelling, mesh, convergence

1. Introduction

Among next generation technologies, a polymer electrolyte membrane (PEM) fuel cell is thought to be a prevalent method for electricity generation having its widespread use across all applications in the near future. Due to its high efficiency and environmental friendliness, this technology is favoured by automotive engineers and scientists and therefore regarded as the most promising candidate that will replace internal combustion engines (ICE) in the transport sector. However, there remain technical challenges such as durability, performance, and cost-effective manufacturing method [1], [2] that need to be addressed in order to bring it to commercialisation.

With the availability of powerful computers, PEM fuel cell modelling has been favoured over experiment in the past few decades as a method to understand the multi-physics inside a PEM fuel cell. Particularly, it is a major tool during the design process to down-select possible designs or operating scenarios that would normally require an expensive and time-consuming testing. However, it should not be misled that PEM fuel cell modelling is a substitute to experiments and they complement each other in the design process.

The two most notable and earliest models were proposed by Springer *et al*. [3] and Bernadi *et al*. [4], [5]. In those one-dimensional models, the transport of reactant species varies in the through-plane direction while the variation along the channel is neglected. Using a mechanistic approach, the transport of chemical species are represented as diffusive and convective fluxes. The so-called membrane water content, λ, on the other hand, is a function of water activity through an empirical relationship derived by Zawodzinski *et al*. [6]. Though being one-dimensional in nature, those models served as a stepping stone for later multi-dimensional models.

The use of a single-domain approach, where boundary conditions are applied only on external boundaries, in electrochemical systems was reported in [7], [8]. Using this approach, Gurau *et al*. [9] later developed a two-dimensional model which led to the first CFD modelling of a PEM fuel cell. The first full three-dimensional model was developed in the work of Dutta *et al*. [10]. In their model, a commercial CFD code was used to solve for the flow-field in a single-channel cell. The user-defined sink and source terms were used to account for species consumption and generation due to an electrochemical reaction, respectively. As a consequence, this has spurred the use of CFD as a major tool to investigate a PEM fuel cell in many aspects.

In the same way as measuring techniques are important to an experiment, thorough understanding of the numerical aspects of a model is critical for a successful CFD simulation. From a model validation perspective, Ju and Wang [11] showed that two entirely different cells operated under the same operating condition could give

exactly the same averaged current density by simply adjusting two basic parameters – exchange current density of oxygen reduction reaction and ionic resistance in the catalyst layer. They then concluded that a polarisation curve was not sufficient to ensure the accuracy of the predicted results and emphasised the necessity of using the local distribution of flow-field variables. Arvay *et al*. [12] attempted to establish the convergence criteria for a PEM fuel cell CFD model. They suggested that the steadiness of important variables should be used alongside the residuals plot in judging convergence and found that at least 15,000 iterations were needed. The generality of their proposed criteria is, however, doubtful.

A survey on PEM fuel cell CFD modelling suggests that typical three-dimensional single-channel models involve at least 10^4 cell elements [13], [14] and this can increase by many folds if more than one channels are included. For a laboratory-scale cell having an active area between 25-100 cm^2, the number of elements can easily reach 10^6 [11], [15]–[18]. Combined with extra equations for a multi-species, two-phase, non-isothermal flow problem, this can be extremely computationally intense. Since the computational resource in terms of CPU power or cores is limited, an effective mesh that gives accurate results while keeping the number of elements to a minimum is therefore needed. In contrast to other engineering flow problems, there are no specific rules on how to mesh a PEM fuel cell. The mesh is usually treated with different strategies depending on the researcher's own experience on PEM fuel cell modelling and is only discussed briefly in their work. As a result, various mesh techniques can be found in the literature – entirely hexahedral, entirely tetrahedral, or the combination of the two, uniform and non-uniform mesh elements, or conforming and non-conforming mesh.

To the best of the authors' knowledge, no study on mesh strategy specifically designed for a PEM fuel cell model has ever been reported. It is therefore the objective of this study to investigate the effect of different mesh strategies on the accuracy of predicted flow-fields in a systematic manner and propose such strategy so it can be used as a guide-mesh in any typical PEM fuel cell simulation. This article is organised in four parts; Part 1 gives the background knowledge on PEM fuel cell modelling and discusses the need for an effective mesh strategy. Part 2 addresses the methodology used to seek for the best mesh strategy where the results are presented and discussed in Part 3. Finally, the mesh strategy is proposed and a conclusion is drawn in Part 4.

2. Methodology

A representative section of a single-serpentine flow-field consisting of two straight channels connected by a 180-degree bend is used. The computational domain consists of anode/cathode flow channels, gas diffusion layers (GDLs), catalyst layers (CLs), and a polymer electrolyte membrane (PEM) as shown in Figure 1 while its dimensions are summarised in Table 1. To aid in the visualisation and discussion of the results, direction convention based on the Cartesian coordinate system is defined as follows;

- The x-axis is referred to as the in-plane (lateral) direction.
- The y-axis is referred to as the along-the-channel (axial, streamwise) direction.
- The z-axis is referred to as the through-plane (cell thickness) direction.

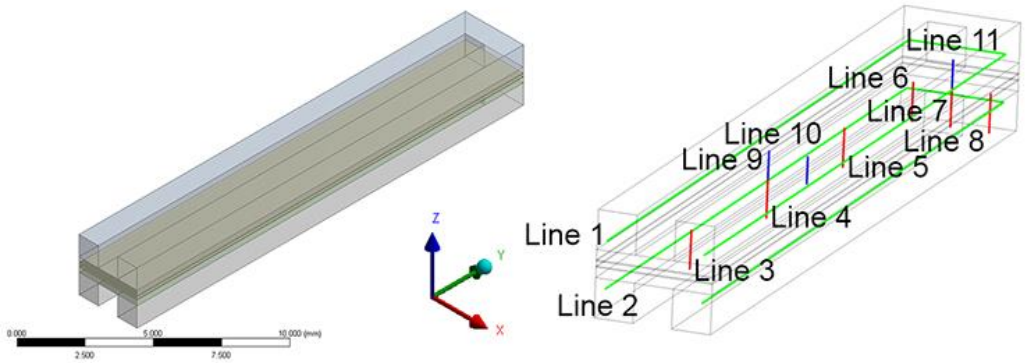

Figure 1: A 180-degree U-bend and pre-defined lines for results visualisation and discussion.

Table 1: Cell dimensions and mechanical properties.

Parameter	Value
Channel width (mm)	1
Channel depth (mm)	1
Rib width (mm)	1
Channel length (from inlet to bend, mm)	20
Active area (cm^2)	0.6
GDLs thickness (μm)	260
CLs thickness (μm)	28
PEM (Nafion 115) thickness (μm)	127
GDLs porosity	0.5
CLs porosity	0.82
Specific surface area of CLs (m^{-1})	1.25×10^7

Since there is no concrete rule on how to mesh a PEMFC computational domain, the most common mesh found in the literature is selected as a "guide mesh". The mesh in each direction will then be coarsened or refined in order to investigate its effect accordingly. All meshes and any modification made to the mesh must comply with the following "mesh etiquette."

- A laminar flow is assumed (a very fine mesh is not needed in the near-wall regions.)
- Structured, hexahedral mesh elements are employed throughout.
- Low (0) skewness and high (1) orthogonality for each cell for good convergence rate.
- Cell aspect ratio is kept below 200 (special care is required in the catalyst layers).
- A large jump in size of adjacent cells is avoided (smooth transition between layers).
- The use of conforming mesh at all interfaces.

The cell is operated under a single-phase flow assumption. The anode and cathode streams are humidified hydrogen and air, respectively. The governing equations used in this study are the ones used and explained in the authors' previous publications [19]–[21] and Fluent Fuel Cells module manual [22] hence not repeated here. The operating conditions are given in Table 2 while properties of all meshes are summarised in Table 3.

Table 2: Operating conditions.

Parameter	Value
Operating temperature (°C)	80
Operating pressure, absolute (atm)	1
Relative humidity for anode gas (RH%)	100
Relative humidity for cathode gas (RH%)	100
Anode gas stoichiometry	3
Cathode gas stoichiometry	3
Anode inlet velocity (ms^{-1}) (corresponding Reynolds number)	0.507 (17)
Hydrogen/water vapour mole fractions for anode gas	0.533/0.467
Cathode inlet velocity (ms^{-1}) (corresponding Reynolds number)	1.207 (47)
Oxygen/water vapour mole fractions for cathode gas	0.112/0.467
Open circuit voltage (V)	1.16

Table 3: Statistics of all meshes presented in this study.

Mesh	Number of Mesh Elements	Orthogonal Quality (avg)	Skewness (avg)	Aspect Ratio (max/avg)
M_1	1 904 000	1	0	12/4
M_2	1 520 000	1	0	7/3
M_3	1 328 000	1	0	5/2
M_4	992 000	1	0	2/1
M_5	952 000	1	0	23/9
M_6	761 600	1	0	29/11
M_7	476 000	1	0	46/18
M_8	190 400	1	0	116/44
M_9	952 000	1	0	23/9
M_{10}	761 600	1	0	29/11
M_{11}	476 000	1	0	46/18
M_{12}	190 400	1	0	116/44
M_{13}	70 720	1	0	54/12
M_{14}	52 864	1	0	107/16
M_{15}	43 936	1	0	199/19

The problem is numerically solved in a commercial CFD code, ANSYS Fluent with a PEM fuel cells add-on module, using SIMPLE algorithm. A point monitor of important variables along with the conservation of mass for reactant species are checked in addition to the residuals plot to ensure a fully converged solution.

3. Results and Discussion

3.1 Through-plane Mesh (Study 1)

From electrochemistry and mass transport viewpoint, the variation of flow-field variables along this direction is critical to current density value. This is the main reason why most early one-dimensional models were developed around this axis assuming zero variation in the other two directions. An accurate solution in the flow channels will ensure accurate reactant species distribution in the porous zones. A typical cross section of the flow channels measures 1×1 mm^2 and is equally divided up using 100 (0.1×0.1 mm^2 each) uniform square elements. As a reference mesh, a $0.05 \times 0.05 \times 0.05$ mm^3 cubical element in the flow channels of Mesh 1 is purposely used. Such fine mesh has not been used anywhere else in the literature except in a micro-channel of a micro PEM fuel cell [23]–[26]. Keeping the mesh in the other two directions the same, the mesh in the porous layers are coarsened. The four meshes and their corresponding polarisation curves are shown in Figure 2.

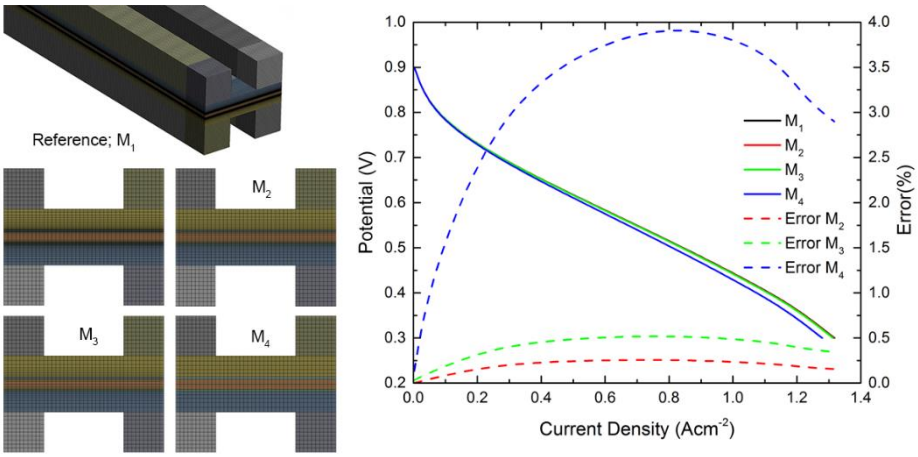

Figure 2: Meshes 1-4 and their corresponding polarisation curves.

The polarisation curves are shown on the right of Figure 2. The percentage errors, as defined in Equation (1), is the percentage deviation of the average current density from the reference value, are also superimposed in the plot. The errors are small at low operating current and increase with the operating current where the maximum error of Meshes 2-4 is found at the mid-current (ohmic) region. Mesh 4, in particular, has only one element in the through-plane direction for both catalyst layers hence giving the highest deviation. This is because its through-plane mesh is not sufficient to accurately resolve the transport of electron in the electronically conductive portion of the porous layers. This also suggests that those early models which treated the catalyst layers as a zero-thickness interface are not a proper representation of a real catalyst layer and thus should be used with care.

$$\%Err = \frac{i - i_{M_1}}{i_{M_1}} \times 100\% \tag{1}$$

For ease of comparison, the operating voltage corresponding to the highest error, 0.30 V, is chosen. Firstly, the local distribution of flow-field variables along the channels is examined. Since the electrochemical reaction takes place in the catalyst layers, the distribution of these variables is susceptible to differ. As can be seen from Figure 3, the differences of velocity and pressure drop among the four meshes are very small. Looking at hydrogen and oxygen mass fractions, it is clear that the effect of a through-plane mesh is more pronounced on these variables which is the result of a non-uniform local reaction rate that varies along the flow path. The deviation not only occurs in the through-plane direction but also in the direction where the flow propagates.

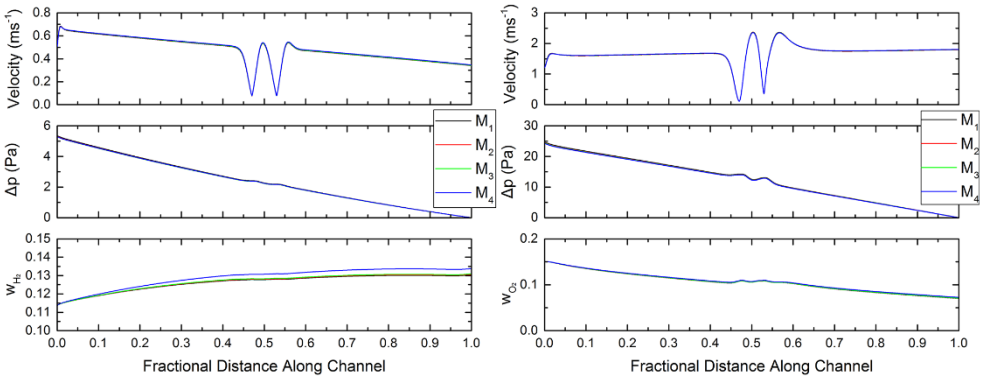

Figure 3: Flow-field variables along the anode (left) and cathode (right) channels.

The velocity profiles across the cathode channel's height at different locations are shown in Figure 4 and Figure 5. Either in the channel or bend regions, there is negligible deviation among the four meshes. Additionally, the asymmetry of the velocity profile about the channel axis can be clearly seen. This is due to different boundary conditions applied at the bottom and top walls of the channel. The non-zero velocity at the top wall is caused by the species flux across this interface into the porous cathode GDL as opposed to the zero velocity at the bottom solid wall where a no-slip boundary condition applies. The oxygen is consumed in the catalyst layer therefore there exist noticeable gradients of oxygen mass fraction both in the through-plane and streamwise directions.

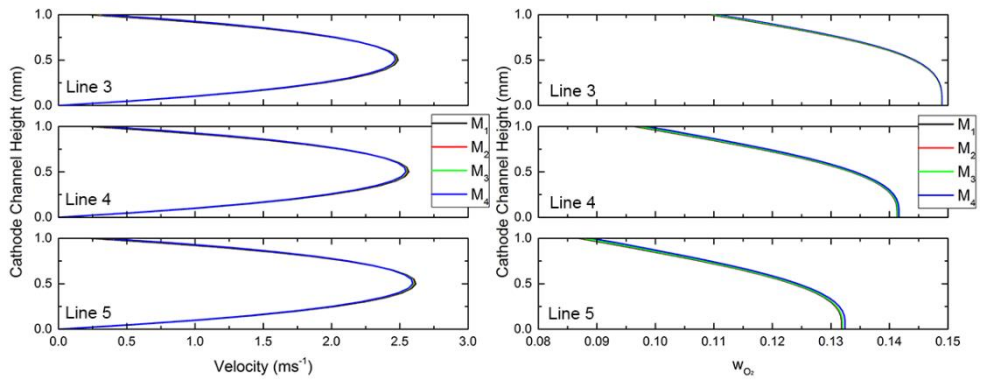

Figure 4: Velocity and oxygen mass fraction across the cathode channel's height in the channel region.

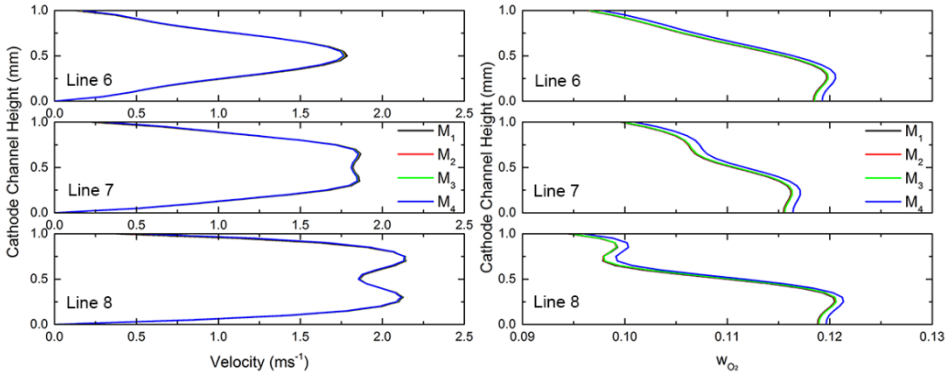

Figure 5: Velocity and oxygen mass fraction across the cathode channel's height in the ben region.

It can be said that the effect of through-plane mesh on the flow-field inside the flow channel is very small and hence negligible. Local distributions of important variables across the porous layers are shown in Figure 6. The low velocity values confirm that diffusion is the dominant transport mechanism in these porous layers in contrast to convection-dominated flow-field in the channels. However, due to a very thin structure of each porous layer, the deviation of Mesh 4 from the other meshes is insignificant even its catalyst layers are coarsest.

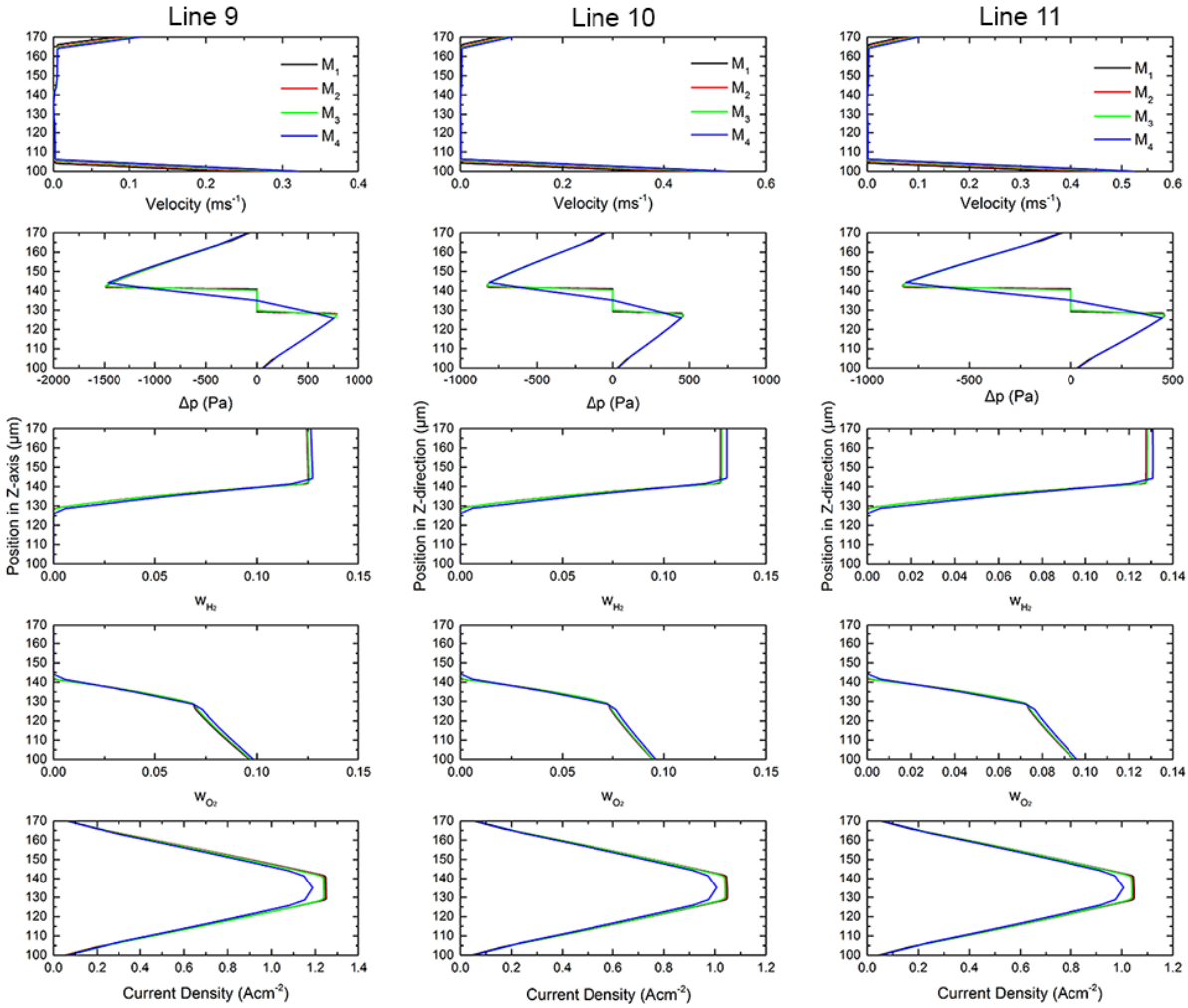

Figure 6: Flow-field variables profiles across porous layers (GDLs/CLs/PEM).

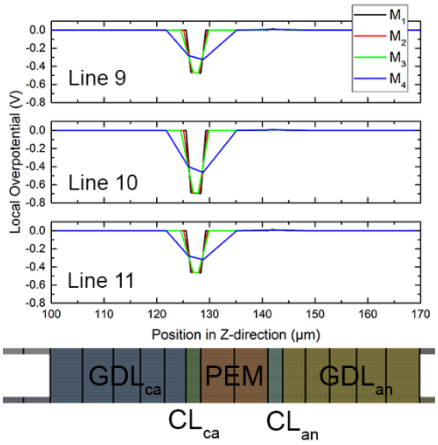

Figure 7: Overpotential profiles across porous layers.

The current density, on the other hand, is not a function of reactant concentrations alone and therefore differs significantly among the four meshes despite similar reactant species distributions. This is confirmed by the profile of an electron-transport-related variable such as local overpotential shown in Figure 7. Clearly, insufficient elements in the porous layers cannot accurately resolve the overpotential. This deviation is further amplified by discrepancies in species distributions resulting in a large current deviation as seen in Figure 2.

3.2 In-plane Mesh (Study 2)

In this study, the effect of the mesh across the width of the cell is investigated by coarsening the mesh in this direction to 0.100, 0.125, 0.200, and 0.500 mm for Meshes 5-8, respectively. The four meshes and their corresponding polarisation curves are shown in Figure 8.

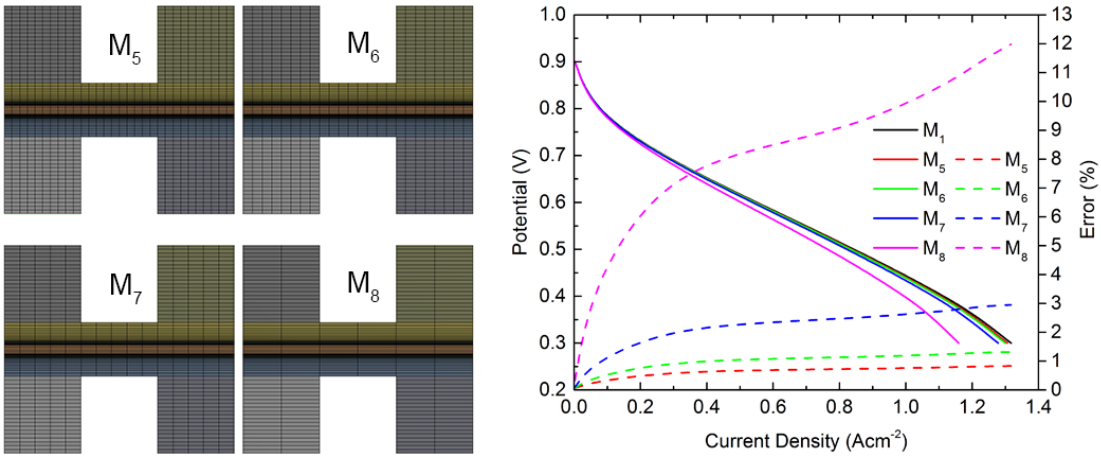

Figure 8: Meshes 5-8 and their corresponding polarisation curves.

The polarisation curves and percentage errors of the five meshes are shown on the right of Figure 8. As expected, the errors increase slightly since there are fewer cell elements in these meshes. However, all error curves are different from those found in Study 1 in which they continually rise with the operating current and the maximum error is found in the mass transfer region with the values of 0.8%, 1.3%, 3%, and 12% for Meshes 5, 6, 7, and 8, respectively. The flow-field of each mesh at 0.30 V is, again, chosen.

Since the lateral mesh is coarsened in this study, a large deviation of flow-field variables in the bend region, where the flow undergoes a drastic 180-degree change in direction, is therefore expected. Nevertheless, an interesting result is found in Figure 9 where velocity profiles of the cathode gas along the three pre-defined lines are shown. There is a negligible difference between the velocities in the bend region in contrast to the ones in the channel region where they differ considerably. This is due to insufficient near-wall cells which cannot accurately resolve the boundary layer in the channel region since the mesh in this area has been coarsened. At the bend, on

the other hand, the direction of the primary flow has changed and therefore its boundary layer is now aligned with the y-axis where the mesh is unchanged. This explains why a large velocity deviation exists in the channel but not in the bend as confirmed by Figure 10. It is evident that the deficiency of near-wall cells causes a larger deviation in velocity profiles across the channel width in the channel region. It should be noted that the large discrepancies in the bend seen in Figure 9 correspond to the entrance and exit of the bend where the flow is influenced by a coarser mesh in the channel.

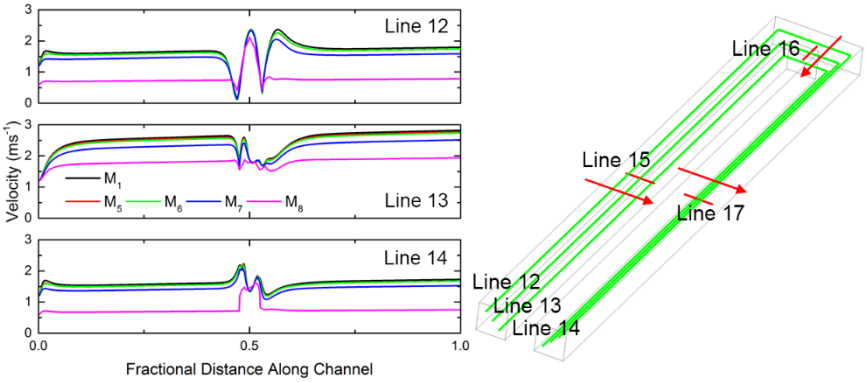

Figure 9: Velocity profiles along the cathode channel. The red arrows indicate the direction vector for the plot.

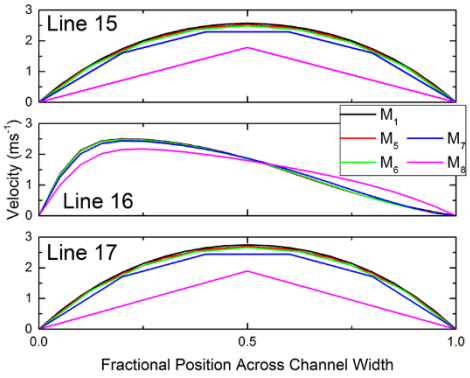

Figure 10: Velocity profiles across the cathode channel width.

3.3 Along-the-channel Mesh (Study 3)

In this study, the mesh in the streamwise direction is investigated. The mesh in the y-direction is stretched to 0.100, 0.125, 0.200, and 0.500 mm in Meshes 9, 10, 11, and 12, respectively. However, the maximum size is limited to 0.500 mm (Mesh 12) to maintain the cell aspect ratio, particularly in the catalyst layers, below 200. The four meshes can be seen in Figure *11*.

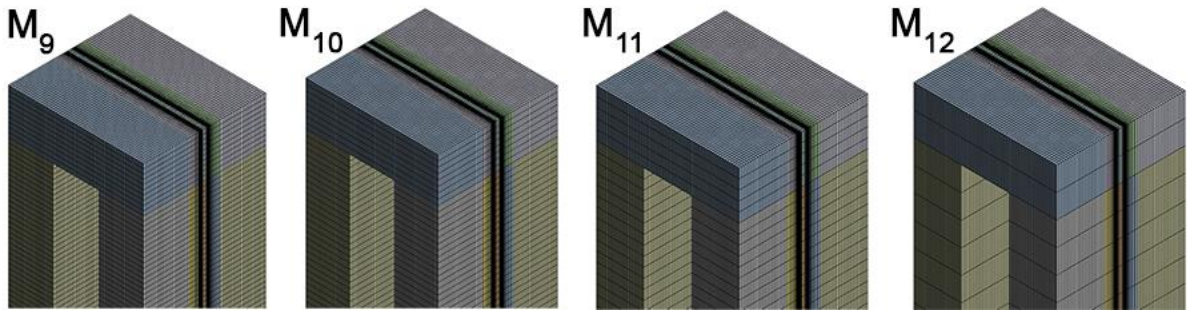

Figure 11: Meshes 9-12.

The four meshes produce impressive results as is evident in Figure 12. The errors are much smaller than those produced by Meshes 5, 6, 7, and 8 despite the fact that the same number of elements are employed. The

errors increase with the current density and the largest deviation of 0.45% is found in Mesh 12 at the highest operating current. Because the y-direction mesh in the bend region is lengthened, a large discrepancy of flow-field variables among the four meshes in this region is seen in Figure 13 where the velocity profiles along Lines 12-14 (defined in Figure 9) at 0.30 V are shown. Clearly, the major source of error of this mesh strategy comes from the bend.

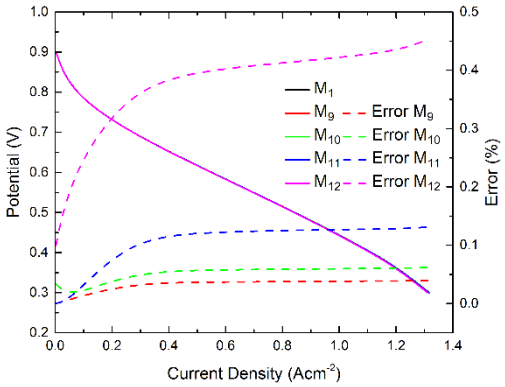

Figure 12: Polarisation curves and percentage errors for Meshes 9-12.

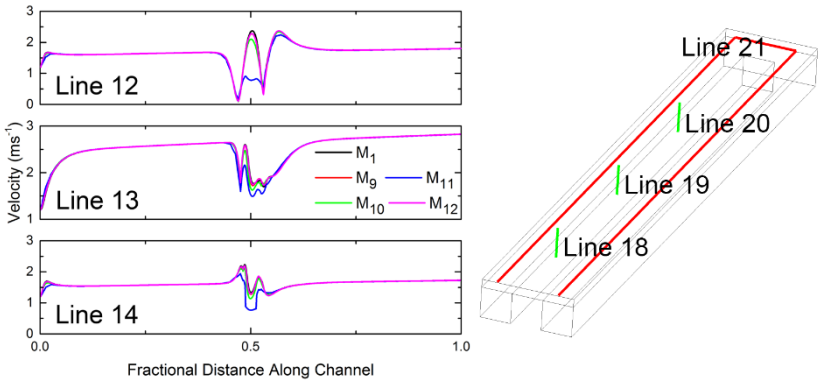

Figure 13: Velocity profiles along the cathode channel.

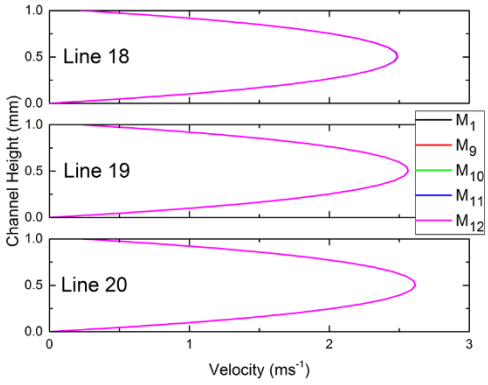

Figure 14: Velocity profiles across the height of the cathode channel at different locations along the channel.

It is clear that the along-the-channel mesh has little effect on the solutions compared to the mesh in the other two directions. This is due to the characteristics of a laminar flow in the flow channels in which the flow reaches its fully-developed stage only a short distance away from the entrance or after it exits the bend. After this point, the velocity field and most flow-field variables remain unchanged and hence the fineness of the mesh in this direction makes no difference as is evident in Figure 14**Error! Reference source not found.** where velocity profiles across the height of the cathode channel are effectively the same regardless of their locations along the channel (Lines 18-20 defined in Figure 13). This is of great benefit since if the streamwise mesh can be relaxed it

will lead to the reduction of total mesh elements considerably. It should be noted that the mesh in this direction cannot be coarsened entirely independently. The reactant gas flow rate, stoichiometric ratio, and other operating conditions play an important role in determining the flow inlet velocity and hence limit the coarseness of such mesh.

3.4 The Proposed Mesh Strategy (Study 4)

In this study, the number of mesh elements are reduced further by employing the strategies found from the previous three studies. A good balance between mesh density and degree of accuracy of Mesh 3 makes it a good platform onto which modifications in the in-plane and along-the-channel directions are made. A uniform value of 1.25 mm in-plane mesh (Mesh 6) is used. This is because the percentage error of 1.3% from this mesh is acceptably low even though it is the highest in Study 2. The biased mesh, nevertheless, is used in the axial direction having dense mesh at the channel inlet/outlet and bend while the mesh in the channel region is coarser. This offers a two-fold benefit. Firstly, at regions where the primary flow undergoes acceleration and deceleration such as channel inlet/outlet and bend entrance/exit, a denser grid will help resolve the flow-field in these regions with greater accuracy. The second benefit is that sufficient near-wall elements are present in the bend. The use of thicker through-plane elements in porous layers allows the axial mesh to be stretched further so that the longest element in Meshes 13, 14, and 15 measures 0.50, 1.00, and 1.77 mm, respectively as shown in Figure 15.

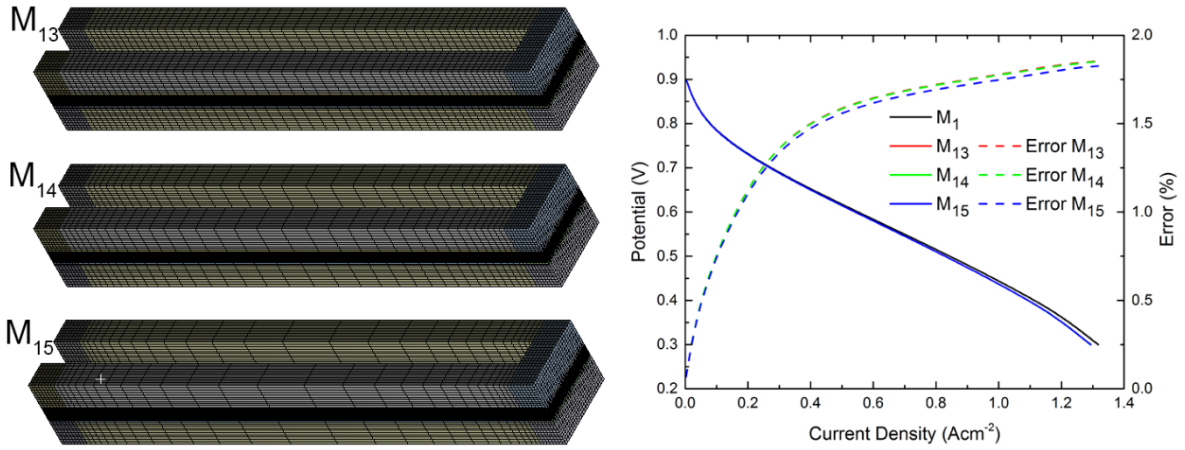

Figure 15: Meshes 13-15 and their corresponding polarisation curves.

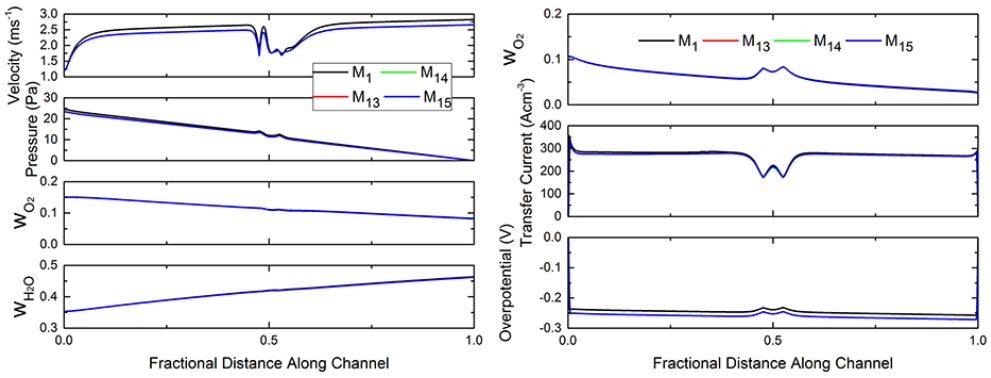

Figure 16: Variables along Line 13 (left, defined in Figure 9) and Line 21 (right, defined in Figure 13).

The polarisation curves on the right of Figure 15 show that the percentage errors are increased as expected. Flow-field variables in the mid-cathode channel along Line 13 and Line 21 are shown in Figure 16**Error! Reference source not found.**. It is evident that three meshes are capable of capturing the characteristics of the profiles from Mesh 1 reasonably well without the presence of large deviation in neither channel nor bend regions. Despite of a slight decrease in accuracy, if the number of mesh elements is taken into account, for example, the reduction of Mesh 15 from Mesh 1 is;

$$\frac{n_{M1}}{n_{M15}} = \frac{1\,904\,000}{43\,936} \times 100\% = 4333\%$$

This 43 times reduction in the number of mesh elements has a penalty of less than 2% error throughout the operating range while characteristics of the flow in all regions are well reserved. This confirms the applicability of the proposed mesh strategy.

3.5 Range of Applicability (Study 5)

In the first part of this study, the U-cell is expanded to form a square cell with an active area of 21×21 mm^2 to prove that the proposed mesh strategy is valid regardless of the cell size. The cell is then meshed using three different mesh schemes as used in Mesh 1, Mesh 4 (zero-thickness CLs), and Mesh 15 (proposed) resulting in 13 028 800, 6 317 200, and 310 144 mesh elements which are referred to as Grids 1, 2, and 3, respectively.

The polarisation and percentage error of the three grids are presented in Figure 17. Each error curve shows its mesh-specific characteristics found in the previous studies despite the fact that they are applied on the new cell. It should be noted that the error from Grid 3 is increased slightly from Mesh 15 as expected due to a larger computational domain. It is interesting to see that the maximum error from Gird 3 (much fewer mesh elements) is almost four times lower than that of Grid 2, indicating that a denser mesh does not always guarantee a more accurate solution if those extra elements are not placed in the correct regions.

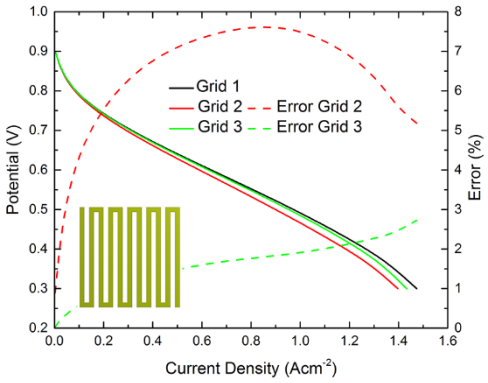

Figure 17: Polarisation and percentage error curves of the square cell under three different grids.

In this second part, the validity of the proposed mesh on different flow-field configurations is tested and presented in Figure 18 showing the polarisation and percentage error curves of parallel and interdigitated cells both having an 11×11 mm^2 active area. Similarly, the error from each mesh scheme follows its unique pattern regardless of the flow-field configurations being used and stays acceptably low. The results from the two parts suggest that the proposed mesh strategy is valid regardless of cell size or flow-field configuration.

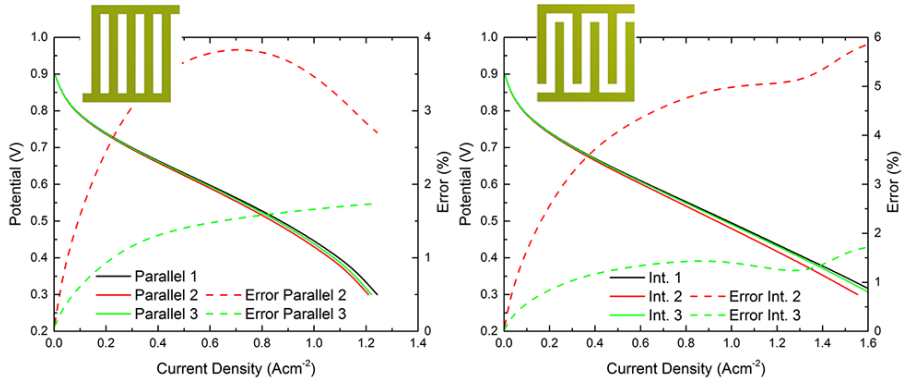

Figure 18: Polarisation and corresponding percentage error curves of the square cell with parallel (left) and interdigitated (right) flow-fields.

4. Conclusion

A three-dimensional CFD model of a PEM fuel cell has been used to systematically investigate the effect of mesh in each direction on the accuracy of the solution. Such effect in each direction is summarised as follows;

- The through-plane mesh has the strongest effect on the accuracy of the solution, especially those electron-transport-related variables, in spite of the least dimension of the cell in this direction.
- The in-plane mesh is responsible for solving the boundary layer at the channel walls and has a moderate effect on the solution and hence sufficient near-wall elements must always be used.
- The axial mesh has the least effect on the solution which offers a great advantage from a computational viewpoint. The mesh in this direction can be relaxed with minimum penalty on the solution accuracy.

Finally, the applicability of the proposed mesh strategy is verified. It proves to be capable of reducing the computational time considerably while giving an acceptable level of accuracy for a wide range of cell sizes and flow-field configurations under typical operating conditions and can be used as a guidance in the meshing process for those who are new to PEM CFD modelling.

5. References

[1] Y. Wang, K. S. Chen, J. Mishler, S. C. Cho, and X. C. Adroher, "A review of polymer electrolyte membrane fuel cells: Technology, applications, and needs on fundamental research," *Appl. Energy*, vol. 88, no. 4, pp. 981–1007, 2011.

[2] K. E. Martin, J. P. Kopasz, and K. W. McMurphy, "Status of fuel cells and the challenges facing fuel cell technology today," *ACS Symp. Ser.*, vol. 1040, pp. 1–13, 2010.

[3] T. E. Springer, T. a. Zawodzinski, and S. Gottesfeld, "Polymer electrolyte fuel cell model," *J. Electrochem. Soc.*, vol. 138, no. 8, pp. 2334–2342, 1991.

[4] D. M. Bernardi and M. W. Verbrugge, "A Mathematical Model of the Solid-Polymer-Electrolyte Fuel Cell," *J. Electrochem. Soc.*, vol. 139, no. 9, pp. 2477–2491, 1992.

[5] D. M. Bernardi and M. W. Verbrugge, "Mathematical model of a gas diffusion electrode bonded to a polymer electrolyte," *AIChE J.*, vol. 37, no. 8, pp. 1151–1163, 1991.

[6] T. A. Zawodzinski, M. Neeman, L. O. Sillerud, and S. Gottesfeld, "Determination of water diffusion coefficients in perfluorosulfonate ionomeric membranes," *J. Phys. Chem.*, vol. 95, no. 15, pp. 6040–6044, Jul. 1991.

[7] W. B. Gu, C. Y. Wang, and B. Y. Liaw, "Micro-Macroscopic Coupled Modeling of Batteries and Fuel Cells: II. Application to Nickel-Cadmium and Nickel-Metal Hydride Cells," *J. Electrochem. Soc.*, vol. 145, no. 10, pp. 3418–3427, 1998.

[8] C. Y. Wang, W. B. Gu, and B. Y. Liaw, "Micro-Macroscopic Coupled Modeling of Batteries and Fuel Cells: I. Model Development," *J. Electrochem. Soc.*, vol. 145, no. 10, pp. 3407–3417, 1998.

[9] V. Gurau, H. Liu, and S. Kakac, "Two-Dimensional Model for Proton Exchange Membrane Fuel Cells," *AIChE J.*, vol. 44, no. 11, pp. 2410–2422, 1998.

[10] S. Dutta, S. Shimpalee, and J. W. Van Zee, "Three-dimensional numerical simulation of straight channel PEM Fuel Cells," *J. Appl. Electrochem.*, vol. 30, pp. 135–146, 2000.

[11] H. Ju and C.-Y. Wang, "Experimental Validation of a PEM Fuel Cell Model by Current Distribution Data," *J. Electrochem. Soc.*, vol. 151, pp. A1954–A1960, 2004.

[12] A. Arvay, A. Ahmed, X.-H. Peng, and A. M. Kannan, "Convergence criteria establishment for 3D simulation of proton exchange membrane fuel cell," *Int. J. Hydrogen Energy*, vol. 37, no. 3, pp. 2482–2489, 2012.

[13] Y. Wang, S. Basu, and C.-Y. Wang, "Modeling two-phase flow in PEM fuel cell channels," *J. Power Sources*, vol. 179, pp. 603–617, 2008.

[14] J. E. Dawes, N. S. Hanspal, O. a. Family, and a. Turan, "Three-dimensional CFD modelling of PEM fuel cells: An investigation into the effects of water flooding," *Chem. Eng. Sci.*, vol. 64, pp. 2781–2794, 2009.

[15] S. Shimpalee, V. Lilavivat, J. W. Van Zee, H. McCrabb, and a. Lozano-Morales, "Understanding the effect of channel tolerances on performance of PEMFCs," *Int. J. Hydrogen Energy*, vol. 36, no. 19, pp. 12512–12523, 2011.

[16] B. Ramos-Alvarado, A. Hernandez-Guerrero, D. Juarez-Robles, and P. Li, "Numerical investigation of the performance of symmetric flow distributors as flow channels for PEM fuel cells," *Int. J. Hydrogen Energy*, vol. 37, no. 1, pp. 436–448, 2012.

[17] S. Jang, G. Shin, H. Hwang, K. Choi, and H. Kim, "Numerical Studies of PEM Fuel Cell with Serpentine Flow-Field for Sustainable Energy Use," in *World Renewable Energy Congress*, 2011, pp. 1205–1210.

[18] P. K. Sinha, C.-Y. Wang, and U. Beuscher, "Transport Phenomena in Elevated Temperature PEM Fuel

Cells," *J. Electrochem. Soc.*, vol. 154, no. 1, pp. B106–B116, 2007.
[19] P. Choopanya and Z. Yang, "Transient Performance Investigation of Different Flow-field Designs of Automotive Polymer Electrolyte Membrane Fuel Cell (PEMFC) Using Computational Fluid Dynamics (CFD)," in *10th International Conference on Heat Transfer, Fluid Mechanics and Thermodynamics 14th-16th July*, 2014, pp. 583–592.
[20] P. Choopanya and Z. Peng, "An investigation on steady-state performance of conventional and serpentine flow-fields for automotive polymer electrolyte membrane fuel cell," in *1st SCODECE Internal Conference (2012 International Forum on Vehicle Control)*, 2012, p. 59.
[21] P. Choopanya and Z. Yang, "A CFD Investigation of Effects of Flow-field Geometry on Transient Performance of an Automotive Polymer Electrolyte Membrane Fuel Cell," *Comput. Therm. Sci. An Int. J.*, vol. 7, no. 2, pp. 93–104, 2015.
[22] ANSYS Inc., "ANSYS FLUENT 12.0 Fuel Cells Module Manual," 2009.
[23] A. S. Rawool, S. K. Mitra, and J. G. Pharoah, "An investigation of convective transport in micro proton-exchange membrane fuel cells," *J. Power Sources*, vol. 162, no. 2 SPEC. ISS., pp. 985–991, 2006.
[24] I. Zahi, C. Rossi, and V. Faucheux, "Micro PEM fuel cell current collector design and optimization with CFD 3D modeling," *Int. J. Hydrogen Energy*, vol. 36, no. 22, pp. 14562–14572, 2011.
[25] J. E. Steinbrenner, E. S. Lee, C. H. Hidrovo, J. K. Eaton, and K. E. Goodson, "Impact of channel geometry on two-phase flow in fuel cell microchannels," *J. Power Sources*, vol. 196, no. 11, pp. 5012–5020, 2011.
[26] S.-W. Cha, R. O'Hayre, S. J. Lee, Y. Saito, and F. B. Prinz, "Geometric Scale Effect of Flow Channels on Performance of Fuel Cells," *J. Electrochem. Soc.*, vol. 151, no. 11, p. A1856, 2004.